THE JOURNAL OF
PHYSICAL CHEMISTRY A

Cryogenic Infrared Action Spectroscopy Fingerprints the Hydrogen Bonding Network in Gas-Phase Coumarin Cations

Eduardo Carrascosa,[‖] Robert P. Pellegrinelli, Thomas R. Rizzo, and Mark A. Muyskens*[,‖]

Cite This: *J. Phys. Chem. A* 2020, 124, 9942−9950

Read Online

ACCESS | Metrics & More | Article Recommendations | Supporting Information

ABSTRACT: We report cryogenic vibrational spectra of gas-phase cations of two common hydroxycoumarins, scopoletin and esculetin, as well as their glycosidic derivatives, scopolin and esculin. The study allows direct observation of the intramolecular interactions between the hydroxyl groups of these molecules. We use cryogenic messenger-tagging IR action spectroscopy to detect vibrational bands in the 3100−3800 cm^{-1} spectral range and discuss the corresponding structural characteristics and hydrogen bonding networks that they imply. The experimental data are supported by a thorough computational evaluation, including investigation of the conformational space. Through comparison of the calculated conformers with the experimental results, we identify the main types of OH oscillators and infer how protonation and sodiation affect the structural arrangement of these molecules. The results presented here provide direct evidence of how slight structural differences sensitively affect the hydrogen bonding network in coumarin derivatives.

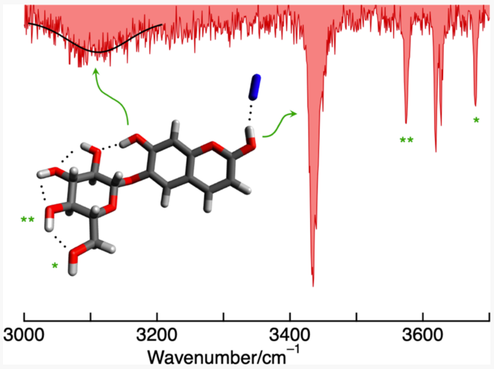

INTRODUCTION

The extensive family of coumarin compounds has attracted attention because of the combination of their fluorescence photoactivity and wide-ranging bioactivity. In many cases, their fluorescence characteristics make them attractive as chemosensors[1] because of not only their high fluorescence quantum yield and large Stokes shift, but also their good photostability and biocompatibility. Natural coumarins often play a protective role in plants,[2] exemplified by the function of scopoletin as an antifungal agent in *Platanus x acerifolia*.[3] Among the many properties attributed to coumarins are anticancer, anticoagulant, antioxidant, antifungal, and antiviral activities.[4−6] Furthermore, some coumarins serve a pharmacological function in humans, perhaps the most well-known of which is the widely prescribed anticoagulant, coumadin.[7]

Esculetin and scopoletin (6,7-dihydroxycoumarin and 6-methoxy-7-hydroxycoumarin, see Scheme 1), investigated in this work, behave both as photoacids and strong fluorophores, as shown for scopoletin in our recent report.[8] Photoacids are considerably more acidic in the electronic excited state than in their ground state, and thus hydrogen bonding can play a significant role in photodynamic processes, especially excited-state proton transfer to the solvent. The photoacidic character is directly tied to the OH in position 7 (OH7), which is a key structural feature that these two coumarins share with umbelliferone (7-hydroxycoumarin).[9] Simkovitch et al.[10] have proposed that the photoacid nature of OH7 in umbelliferone is directly related to its bioactivity. With an additional oxygenated substituent on the benzene ring, both esculetin and scopoletin can exhibit an intramolecular hydrogen bond from OH7 to O6. Thus, knowing more about the nature of this hydrogen bond aids understanding of these two coumarins.

There are naturally occurring glycosidic derivatives of esculetin and scopoletin, namely, esculin and scopolin, respectively (Scheme 1). Replacing the glucopyranosyl group with a hydrogen converts the glycoside into its aglycone. Of the four coumarins shown in Scheme 1, scopolin is the only one that is relatively nonfluorescent and lacks an ionizable proton in position 7. The review by Duval and Duplais[11] describes scopoletin and scopolin as having beneficial bioactivity and scopoletin with useful fluorescent properties to probe stress response and localization in cells. Tattini and co-workers[12] have recently reviewed the effective antioxidant activity of esculetin as a stress response in plants. Their study highlighted the beneficial role of esculetin and esculin as photoprotective, UV-B absorbers. The anti-inflammatory function of esculin is further discussed in the review by Kirsch et al.[6] While all these reports emphasize important macroscopic properties, they lack a molecular-level understanding that may provide structure−activity relationships for these species.

Received: July 14, 2020
Revised: November 5, 2020
Published: November 17, 2020

https://dx.doi.org/10.1021/acs.jpca.0c06430

Scheme 1. Coumarins Investigated in This Work, Including Conventional Carbon Numbering for Coumarin and Glucopyranose Structures

Name	R(7)	R'(6)
esculetin, Et	OH	OH
scopoletin, St	OH	OCH_3
esculin, En	OH	βDg
scopolin, Sn	βDg	OCH_3

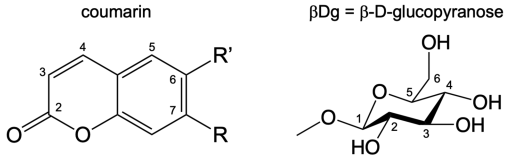

In the last decades, gas-phase spectroscopy and dynamics investigations have been established as the methods of choice to unravel fundamental inter- and intramolecular interactions in isolated molecules, thus providing atomic-level understanding for observations in complex environments.[13,14] State-of-the-art action spectroscopy, more specifically cryogenic ion spectroscopy, has recently emerged as a powerful method to unravel structural and photophysical properties in molecular species of a wide size range, often providing a direct comparison with computational predictions.[15] This technique has been particularly relevant for studying complex biomolecules because of its ability to distinguish even the subtlest structural patterns.[16] In particular, the development of cryogenic messenger-tagging infrared action spectroscopy has facilitated the study of complex molecular ions in the gas phase, avoiding complications associated with thermal broadening present in spectra taken at room temperature as well as the nonlinear effects of infrared multiphoton dissociation.[17−21]

This report presents cryogenic messenger-tagging infrared action spectra of eight gas-phase coumarin cations (the four coumarins shown in Scheme 1 as both protonated and sodiated species), including an assignment of the main structural patterns, and highlights a range of hydrogen bonding features. The cationic forms in the aqueous phase play a negligible role over the pH range 2 to 12, where the acid−base equilibria of the neutral, tautomer, and anion forms are key to the photoacid behavior. For example, the umbelliferone cation exists only below pH 0.[9] These results for the cations allow fingerprinting the structure of each species and provide a direct benchmark for computational studies.

■ METHODS

Experimental Approach. To determine the structure of the coumarin cations, cryogenic infrared action spectra were obtained in the OH stretch region (3100−3800 cm^{-1}) using a tandem quadrupole mass spectrometer containing a cryogenic, octupole ion trap, which has been described in detail elsewhere.[22] Briefly, each target species was dissolved at 0.1 mM in a water−methanol (1,1) mixture and brought into the gas phase via nanoelectrospray ionization (nESI). Trace concentrations of acetic acid and sodium acetate were added to the solutions to generate protonated and sodiated coumarins, respectively. After nESI, the gas-phase ions were radially confined in a radio-frequency driven ion funnel and transferred into a hexapole guide, where they were trapped and eventually extracted as 120-μs packets into a first quadrupole mass filter at a repetition rate of 10 Hz. Passing through the quadrupole, the ion species of interest was selected and further guided through two electrostatic benders and an octupole ion guide into a linear octupole ion trap attached to a cryogenically cooled copper housing. Here, ions were thermalized with a precooled He or N_2 buffer gas, which was previously introduced via a pulsed valve to the trap region in pulses of ∼300 μs duration. For the N_2 messenger-tagging experiments, the trap was held at 50−60 K, while the He tagging experiments were carried out at 4.5 K. The temperature was read out using a silicon diode (LakeShore Cryogenics DT-670) attached to the copper trap housing and maintained through implementation of a 50-Watt heater and a PID controller.

In order to obtain single-photon infrared spectra at cryogenic temperatures, the target ions were "tagged" during their residence time of 95 ms in the trap, whereby one or more of the N_2 or He buffer gas molecules formed weakly bound complexes with the coumarin cations. The trapped messenger-tagged ions were then irradiated with tunable infrared light from a pulsed optical parametric oscillator (LaserVision). In the event of a resonant vibrational excitation, the tagged ion was excited and relaxed through intramolecular vibrational energy redistribution, thereby detaching the weakly bound tag and forming the bare ion. All resulting ions were then extracted out of the trap into a second quadrupole mass filter and finally detected using a Channeltron ion detector. By selecting the ion mass associated with the messenger-tagged coumarin and monitoring its depletion as a function of the infrared wavenumber in a *light on* minus *light off* experiment, the resulting cryogenic infrared action spectra were obtained. The spectrum was power normalized to account for the differences in OPO light fluence during the scan.

While esculetin and scopoletin are rigid, planar molecules, introducing a proton or sodium ion into the system can potentially result in different protomers or sodium positional isomers. For scopolin and esculin, additional rotation about the glycosidic bond can result in the presence of multiple stable conformers. Furthermore, different clockwise and counterclockwise configurations of the hydroxyl groups in the glycoside might co-exist. To investigate the existence of multiple isomers in the gas phase for each of the studied species, the same solutions were electrosprayed into a recently developed ultra-high-resolution ion mobility mass spectrometer.[23] The ion mobility device allows for separation path lengths of tens of meters and has demonstrated its ability to separate even structurally analogous saccharide anomers. Thus, structural differences such as those promoted through the rotation of the glycosidic bond should be well-resolved. Importantly, the obtained arrival time distributions showed a single peak for all glycoside ions studied in this work even after ion mobility path lengths of over 27 meters (see Figure S1 for an example). This is consistent with the number of observed infrared bands, which in each case matches the number of OH oscillators for a single species (see below). However, it cannot be completely ruled out that the observed ion mobility peak consists of two or more rapidly interconverting conformers.[24] Even though this situation is possible (if the isomerization barriers are low enough), the experimental width of the infrared transitions, in particular in the free OH stretch region, is linewidth-limited, making the presence of rapidly interconverting isomers unlikely.

Computational Methods. To support our experimental findings, we performed electronic structure and vibrational frequency calculations on all the target ions, including a thorough evaluation of the conformational space for each species. The calculations were done using the Gaussian 16 program package[25] and the WebMO Pro interface.[26] We follow a number of studies on closely related molecular systems, for example, gas-phase *β*-phenylglucoside,[27,28] which base their modeling approach on the hybrid functional B3LYP.[29−31] Unless otherwise noted, we use the cc-pVDZ Dunning basis set (DZ). Our modeling approach comprises the B3LYP/DZ level of theory for geometry optimization and determination of harmonic frequencies, intensities, and zero-point energies, followed by single-point energy calculation using the Møller-Plesset perturbation theory (MP2). Because the B3LYP is known to be somewhat deficient in accounting for dispersion interactions, we also evaluate selected conformers with the dispersion-corrected functional B97-D3.[32] The basis set superposition error (BSSE) is corrected by using the counterpoise method (CP),[33] treating all noncovalently bound species as individual fragments for all geometry optimizations. Care was taken to ensure that full geometry optimizations for each structure resulted in a global minimum energy, which for the glycosides involved consideration of multiple conformers around the glycosidic bond, different orientations of the sugar hydroxyl, and exocyclic hydroxymethyl groups, as well as different interaction patterns with Na^+ when present. To assess the dependence of the relative energies on the level of theory, single-point, BSSE-corrected calculations were performed at the following additional levels, B97-D3/cc-pVDZ, M06-2X/cc-pVDZ, and B3LYP/6−311++G(2d,2p), for selected conformers of EnH^+, SnH^+, and $SnNa^+$ (Table S3).

For comparison of calculated frequencies with the experimental spectrum, we use a scaling factor. The data set used to determine the NIST compiled[34] scaling factors includes very few OH stretches, which likely means the scaling factor does not adequately represent the region of OH stretches relevant to this work. Our scaling factor optimizes the agreement of nine B3LYP/DZ calculated frequencies corresponding to the two aglycone oscillators attached to the benzene ring, designated as OH6 and OH7, which covers the range 3430 to 3660 cm^{-1}. These are experimental lines for which we have confidence in the spectral assignment and are lines where we expect good agreement between calculation and experiment. Our scaling factor is 0.9654, which is <0.5% smaller than the NIST scaling factor for B3LYP/DZ of 0.970. Because the more red-shifted lines are expected to be less certain, we apply this adjusted scaling factor to all calculated OH frequencies. We determine a similarly optimized scaling factor for B97-D3 calculation results included in the Supporting Information (see notes to Table S1). It is possible that a linear correction to DFT-calculated frequencies similar to the work of Katari et al.[35] may lead to better agreement overall, but a clearer picture of agreement between calculation and experiment for the more strongly hydrogen-bonded interactions and among glycoside conformers is required before this relationship can be established.

■ RESULTS

Aglycone Spectra. Figure 1 shows the infrared (IR) spectra of the four aglycone cations with N_2 tagging, as well as a comparison spectrum of EtH^+ tagged with the much less polarizable He atom. All five spectra show a band near 3550 cm^{-1} associated with the OH7 stretch vibration, which is common to all four cations. The protonated spectra with N_2-tag (Figure 1b,c) possess an OH stretching band near 3400 cm^{-1}, which is not present in the spectra of the sodiated species (Figure 1d,e). This band corresponds to the vibration of the proton attached to the carbonyl oxygen (OH2) and hydrogen-bonded to N_2. Figure 1a,b shows that the N_2 tag shifts one of the three peaks ∼150 cm^{-1} to lower frequency, which clearly indicates that the N_2 tag interacts with OH2. Finally, EtH^+ and $EtNa^+$ both show an additional band compared to their corresponding counterparts, StH^+ and $StNa^+$, near 3650 cm^{-1} because of the presence of the additional OH6 oscillator. These observations are supported by the calculated structures discussed below.

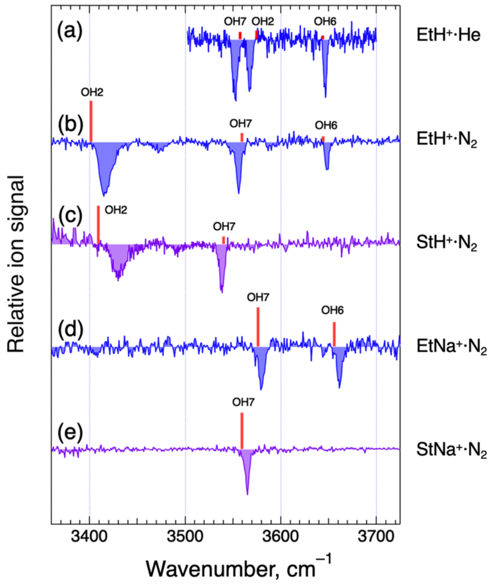

Figure 1. Infrared action spectra of four aglycone cations with calculated OH vibrational frequencies. Solid traces are (a) esculetin-H^+ (EtH^+) tagged with He (the remaining spectra are tagged with N_2), (b) esculetin-H^+ (EtH^+), (c) scopoletin-H^+ (StH^+), (d) esculetin-Na^+ ($EtNa^+$), and (e) scopoletin-Na^+ ($StNa^+$). Sticks are OH vibrational frequencies from B3LYP/cc-pVDZ (BSSE-corrected) models; stick heights represent normalized intensity for each spectrum, except heights for sticks above trace a, which are relative to the largest calculated intensity in trace b for comparison.

Glycoside Spectra. Figure 2 shows the cryogenic IR spectra of the four glycoside cations studied under N_2 tagging conditions. Because the protonated spectra (Figure 2a,b) show a prominent band near 3440 cm^{-1}, not present in the sodiated spectra (Figure 2c,d) and analogous to the band in EtH^+ and StH^+, it is reasonable to deduce that protonation for the glycosides also occurs at the carbonyl oxygen forming OH2, which is influenced by the N_2 tag in a way similar to the aglycone spectra. The spectrum of EnH^+ (Figure 2a) shows six bands: the OH2 band near 3440 cm^{-1}, four peaks above 3550 cm^{-1}, and a strongly red-shifted and broadened peak around 3100 cm^{-1}. Comparing StH^+ (Figure 1c) with SnH^+ (Figure 2b), in which the OH7 is replaced by the glucopyranose moiety, the single peak in the former is replaced in the latter spectrum by four bands located between 3600 cm^{-1} and 3700 cm^{-1}, which represent the four sugar hydroxyl groups. In the case of sodiated esculin ($EnNa^+$, Figure 2c), the five observed bands between 3600 and 3700 cm^{-1} account for all expected

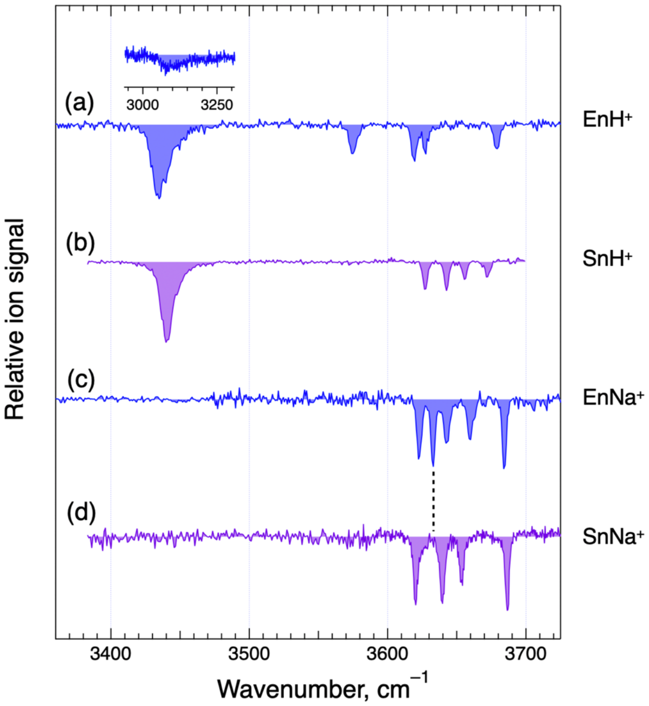

Figure 2. Infrared action spectra of four glycoside cations. Solid traces are (a) esculin-H$^+$ (EnH$^+$) with the inset, (b) scopolin-H$^+$ (SnH$^+$), (c) esculin-Na$^+$ (EnNa$^+$), and (d) scopolin-Na$^+$ (SnNa$^+$), all with a N_2 tag. The dashed line is centered on the 3633 cm^{-1} peak of EnNa$^+$.

OH vibrations. The OH7 band of EnNa$^+$ appears above 3620 cm^{-1} as compared to 3580 cm^{-1} in the aglycone EtNa$^+$ (Figure 1d), suggesting a significant change in its environment. The sodiated scopolin (SnNa$^+$) spectrum (Figure 2d) consists of four bands appearing in the same frequency region as those of EnNa$^+$ and lacks the infrared transition at 3440 cm^{-1} corresponding to the protonated carbonyl in SnH$^+$. The dashed line in Figure 2 is centered on the line at 3633 cm^{-1} in the EnNa$^+$ spectrum, which the theoretical results suggest corresponds to the OH7 oscillator.

Table S1 lists the experimental bands for all eight N_2-tagged cations and He-tagged EtH$^+$. The cryogenic IR spectra in Figures 1 and 2 show clearly resolved vibrational transitions that account in number for the expected OH vibrations for each cation. These uncongested spectra together with the IMS analysis for EnH$^+$ and EnNa$^+$ suggest that we are observing single conformers of these cations, a remarkable observation given the high number of energetically similar conformations found in the present theoretical analysis and because several recent studies on glycans[36] and sodiated glucose[37] under similar conditions contend with the presence of multiple conformers.

■ MODELING

Computational modeling provides further insights into the vibrational assignments and the existence of various types of hydrogen-bonding and other noncovalent interactions present in these structures. Because the experimental data comprise uncongested OH vibrations in the gas phase, we compare them directly with the computationally obtained frequencies after applying the appropriate scaling factor. For each cation, the modeling procedure yields multiple possible conformers; for the aglycones, this amounts to several different orientations of the hydroxyl groups in the coumarin plane, whereas the glycosides present a vast conformational space. A practical measure of spectral agreement between the calculated and experimental spectrum is to calculate the root-mean-square deviation, $\mathrm{RMSD} = \left(\frac{1}{n}\sum_i^n (\nu_i^c - \nu_i^e)^2\right)^{1/2}$, where ν_i^c is the calculated frequency and ν_i^e is the experimental frequency for all n peaks in order of appearance in a spectrum. For the aglycones, the RMSD is a good metric of agreement between experiment and calculation because we have confidence in the spectral assignments. For the glycosides, our confidence in spectral assignments is limited, and in this case, having a low RMSD is a necessary but not sufficient condition to identify the correct conformer. Table S1 also includes the calculated frequencies for selected conformers using two different functionals, B3LYP and B97-D3, showing B3LYP to provide a better model in six of the nine spectral comparisons.

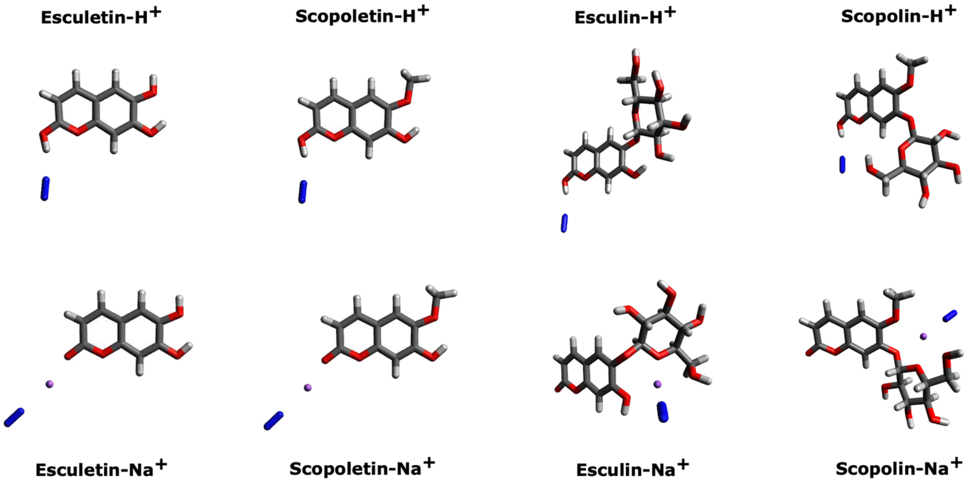

Figure 3. Calculated molecular structures for selected conformers of all eight cations with a N_2 tag at the B3LYP/cc-pVDZ level of theory with BSSE correction. For the aglycones and the esculin cations, they are the lowest energy conformers, and for the two scopolin cations, they are representative conformers as discussed in section Glycoside Conformers. The violet sphere represents the Na$^+$ ion. In the protonated structures, the N_2 tag binds to the proton in the coordinate covalent bond to C=O, and in the sodiated structures, the N_2 tag binds to the Na$^+$ ion.

Aglycone Conformers. Figure 3 shows the lowest energy aglycone conformers calculated at the B3LYP/DZ level of theory. Because the systems described here involve both *intermolecular* and *intramolecular* hydrogen bonds, we adopt the abbreviations IrHB and IaHB to designate the former and latter, respectively. Anticipating the need to distinguish vibrational modes because of hydroxyl groups attached to the coumarin backbone from the glucopyranosyl hydroxyls, we label an OH vibrational band on the coumarin as γn, where n refers to the carbon number to which the OH is attached (see Scheme 2). The red sticks in Figure 1 show the calculated frequencies and relative intensities for the lowest energy conformer in each case, and the labels indicate the number position of the OH on the coumarin structure. The reasonable agreement between measured and calculated spectra supports our suggestion that the $\gamma 2$ band involves an IrHB to N_2 and that $\gamma 7$ involves the IaHB between OH7 and O6. For both esculetin cations, the highest frequency band is assigned to $\gamma 6$, the stretching of the non-hydrogen bonded OH6.

Scheme 2. Labeling of OH Vibrational Modes and Hydrogen Bonds for EtH$^+$ (left) and EnH$^+$ (right, Conformer A in the Supporting Information)[a]

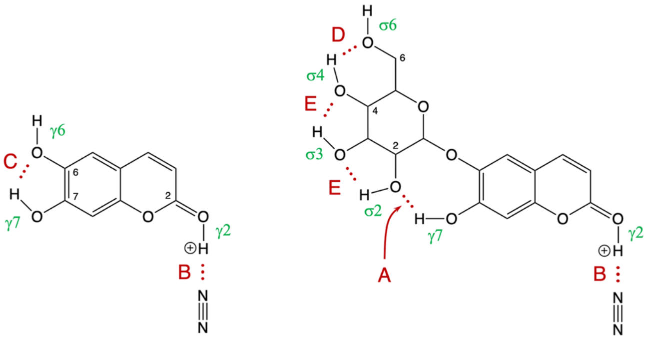

[a] Hydrogen bonds are depicted with red dots and labeled according to the type, as described in the Discussion section

Glycoside Conformers. The substitution of a hydroxyl group with a glucopyranose (GP) ring doubles the number of atoms in the molecule and introduces significant structural flexibility via rotation of the glycosidic linkage between the two ring systems (Scheme S1). Table S3 provides an illustration of the four possible combinations of the GP ring orientation with respect to the coumarin plane in the four lowest energy conformers calculated for EnH$^+$. Because the coumarin and glucopyranose moieties have similar atom numbering schemes, we use a prime (’) to indicate an atom that is part of the GP ring. To distinguish vibrational assignments on the two rings, we label an OH band on the GP ring as σn, where n refers to the carbon number to which the OH is attached, such that $\sigma 6$ is the IR band due to the OH6’ (Scheme 2). In addition, the flexibility of the hydroxyl and hydroxymethyl groups on the GP ring requires consideration of a plurality of possible conformations, although maximizing hydrogen bonding among these groups normally limits them to a much smaller set characterized by a direction labeled clockwise or counterclockwise (Scheme S1). A complete description of the GP ring conformation is described in Scheme S2.

A comprehensive study of conformers for all four glycosides was carried out at the B3LYP/DZ level of theory, taking into consideration configuration of the two ring systems, coordination of oxygen atoms to Na$^+$ when applicable, and the orientation of the hydroxyl and hydroxymethyl groups of the GP ring. Among these conformers, all structures having an energy within 20 kJ/mol of the lowest energy structure received the full hybrid modeling approach that includes zero-point energy correction, BSSE correction, and the MP2 single-point refinement of the energy. In addition to the electronic energy calculations, harmonic vibrational frequencies of each conformer were calculated and compared to the corresponding experimental spectrum. While the calculated lowest energy conformer provides reasonable agreement with the experimental spectrum for EnH$^+$ and EnNa$^+$, this is not the case for SnH$^+$ and SnNa$^+$. For the latter two ions, the conformer that provides the lowest RMSD represents the closest agreement to the experimental spectrum of those found in our conformer search process; these are the scopolin ion conformers shown in Figure 3. Figures S2–S5 show the comparison of calculated spectra of all the glycoside conformers below 20 kJ/mol relative energy to the experimental spectra, and Tables S2 and S4–S6 provide corresponding structural information.

The main findings of the glycoside modeling are as follows: (1) the presence of an IaHB between the coumarin and the glucopyranose in EnH$^+$; (2) the lack of a corresponding IaHB in SnH$^+$, making it similar in structure to a phenyl-tagged glucoside; (3) confirmation of the IrHB of the N_2 tag to the proton on C=O; and (4) a multidentate chelation of the sodium ion in both EnNa$^+$ and SnNa$^+$. The calculated lowest energy EnH$^+$ conformer gives the best agreement with the experimental spectrum. The most red-shifted peak in the spectrum (Figure 2a inset) is assigned to $\gamma 7$, the vibrational stretching of OH7 as a donor to an intramolecular hydrogen bond bridging the two rings. Our modeling also indicates strong coupling of $\gamma 7$ to the coumarin CH5 stretching vibration. The next most red-shifted line in the EnH$^+$ spectrum is assigned to the $\gamma 2$ stretch, which is formed by protonating the carbonyl oxygen and serves as a donor in the IrHB to the N_2 tag, confirming the influence of the N_2 tag in the spectrum.

The four remaining lines in the EnH$^+$ spectrum belong to σ-vibrations and provide a fingerprint to distinguish among conformers. The most red-shifted of these lines (3575 cm^{-1}) stands out in comparison to the other σ-vibrations in the EnH$^+$ spectrum as well as all the σ-vibrations in the other glycoside spectra. The EnH$^+$ conformers that include an IaHB with an OH4’ donor and O6’ acceptor have frequencies that are similarly red-shifted; no other arrangement gives as large a red shift among σ-type hydrogen bonds. What makes this IaHB different from others in the GP ring is that six atoms form the ring closed by the hydrogen bond, allowing a shorter H···O distance hence a stronger HB. The less red-shifted σ-bands involve a more constrained five-member ring closed by a hydrogen bond and have a larger H···O distance. In the EnH$^+$ conformer, $\sigma 4$ is the terminal HB in a chain of four with a clockwise orientation that begins with $\gamma 7$ inter-ring HB (shown in Scheme 2).

The remaining σ-type bands in the EnH+ spectrum form a pattern that is sensitive to the environment of these hydroxyl groups. In the lowest energy conformer, $\sigma 2$ and $\sigma 3$ form a coupled pair with a frequency spacing similar to the observed spectrum. The highest frequency band in the spectrum is assigned to $\sigma 6$, which by comparison to the frequency of a gas-phase alcoholic OH, such as methanol,[38] we deduce to be not hydrogen-bonded.

Table 1. Hydrogen-Bond Characteristics in Coumarin Cations, Sorted by Increasing Donor Frequency[a]

label	donor	acceptor	example	donor OH frequency (cm^{-1})	peak width[b] (cm^{-1})	H···O distance[c] (Å)
A	OH7 on coumarin	O2' on sugar	EnH^+	3100	43	1.7
B	OH2 on coumarin	N on N_2	EtH^+, StH^+, EnH^+, SnH^+	3420−3440	9.5	2.0
C	OH7 on coumarin	O6 on coumarin	EtH^+, StH^+, $EtNa^+$, $StNa^+$	3540−3580	4.1	2.1
D	OH4' on sugar	O6' on sugar	EnH^+ $\sigma4$	3575	4.0	1.9
E	OH on sugar	O on sugar	EnH^+, SnH^+, $EnNa^+$, $SnNa^+$	3620−3680	2.4	2.4

[a] The label in the first column refers to Scheme 2. [b] Width from the gaussian fit and an average value where multiple peaks are involved [c] Atom distances are from the conformers represented in Scheme 2

For the remaining glycosides, which clearly lack the $\gamma7$ IaHB, the modeling search produces conformers with variable results where the lowest energy conformer has reasonable agreement with the IR spectrum for only $EnNa^+$. This reduces our confidence in making specific assignments of σ-type stretches. The spectra of the calculated conformers of SnH^+ feature the expected $\gamma2$ band near 3440 cm^{-1} and a cluster of OH bands from the sugar moiety. The two lowest energy conformers exhibit much poorer agreement with the experimental spectrum compared to conformer with best spectral agreement, which exhibits band positions and intensities that match well with the four nearly equally spaced sugar OH lines (see Figure S3). While the bands between 3600 and 3700 cm^{-1} are clearly σ-lines, only the $\gamma2$ assignment is certain. We also note that both the lowest energy conformer and the one with best spectral agreement appear to be influenced by the presence of the N_2 tag.

With respect to the sodiated glycosides $EnNa^+$ and $SnNa^+$, calculations predict the most stable conformers to have tridentate and tetradentate coordination of oxygen atoms to the sodium ion. In the case of $EnNa^+$, the lowest energy conformer, which is tetradentate, gives the best apparent agreement with the spectrum, consisting of four σ-lines and one $\gamma7$ line (see Figure S4). While the modeling process leaves some uncertainty in the sigma assignments, the $\gamma7$ line is consistently predicted to be around 3630 cm^{-1}, supporting the idea that $\gamma7$ shows up as the second to left peak in the $EnNa^+$ spectrum. The lowest energy conformers of $SnNa^+$, on the other hand, do not present a good match to the experimental data. A conformer that is calculated to be 19 kJ/mol higher in energy than the most stable conformer exhibits the best agreement with the experimental spectra based on the lowest RMSD value (see Figure S5). While kinetic trapping of stable, solvated structures has been observed in previous gas-phase studies,[39] the likelihood of kinetic trapping producing a single conformer in our ion trap seems low and perhaps points as much to inadequacies in the search for conformers and modeling level of theory.

■ DISCUSSION

The experimental IR-spectra of the studied protonated and sodiated coumarin derivatives show well-resolved, characteristic vibrational bands that can be attributed to significantly different bonding arrangements. Detailed structural features can be assigned by comparison between experiment and computational modeling. A first scrutiny of the experimental spectra shows that sodiation and protonation lead to significantly different arrangements of the hydroxyl groups. A proton binds coordinate covalently, forming a bond with any lone pair. While complex protonated species often show the presence of a considerable number of energetically stable protomers, this is not the case for the molecules studied here. In fact, both experiment and theoretical modeling reveal that for all studied protonated molecules, H^+ binds exclusively at the carbonyl group ($C{=}O$) on the coumarin moiety. This manifests as an additional OH stretching vibration in the range of 3400−3450 cm^{-1}. On the other hand, the sodium cation binds only noncovalently and in the case of the glycosides can involve multiple oxygen atoms interacting with the Na^+-positive charge. The IR spectra reveal that the Na^+ binds to the $C{=}O$ of the aglycone but coordinates to multiple oxygen atoms in the glycoside. Similar observations have been reported in recent papers.[40,41]

Theoretical modeling of the eight investigated cation structures supports the identification of five distinct types of hydrogen bonding, labeled in Scheme 2 and listed in Table 1. The EnH^+ structure alone exhibits four of these, while the fifth kind is the IaHB found in all four of the aglycones. As expected, the strong hydrogen bonding characteristics of the lower-energy IR bands result in a significant spectral broadening, while the high-frequency "free" OH oscillators lead to narrow bands. The two highest frequency OH bands, which are on the GP ring of $EnNa^+$ and $SnNa^+$, are observed in the 3684−3686 cm^{-1} range, slightly higher than that of an alcoholic free OH at ~3680 cm^{-1}, and show an average width of 2.0 cm^{-1}, which is near the linewidth limit of our optical parametric oscillator.

As indicated in Scheme 2, hydrogen bond A corresponds to the interring IaHB in EnH^+. For comparison, a recent study of phenyl-lactose (phenyl-β-lactoside)[4] describes hydrogen bonding between two GP rings, which gives red-shifted peaks between 3400 and 3500 cm^{-1}, similar to N_2 binding to OH2 ($\gamma2$) in the protonated coumarins of this work, but not matching the interring 3100 cm^{-1} peak found in EnH^+. The large red shift in EnH^+ implies a uniquely strong hydrogen bond. Hydrogen bond B corresponds to that between the protonated carbonyl and the N_2 tag in all four of the protonated coumarins. This hydrogen bond stands out in our spectra as a strong IrHB based on its red shift, only exceeded by hydrogen bond A. It represents the highly specific localization of the tag in the protonated coumarins.

Hydrogen bond C involves the $\gamma7$ oscillator in all four of the aglycones. This hydrogen bond closes a five-member ring constrained to the coumarin plane involving the two oxygenated benzene ring substituents on the coumarin. Hydrogen bond D corresponds to the unique hydrogen bond in a six-membered ring mentioned in the Results section for EnH^+. The characteristics of this relatively strong, hydrogen bond among the sugar OHs demonstrate that the flexibility of a six-membered ring allows a smaller H···O distance than the constraint of a five-member ring on the sugar and hence a stronger hydrogen bond with a more red-shifted frequency. Scutelnic and Rizzo[43] report a quite similar six-member hydrogen-bonded ring in the two higher energy conformers of protonated glucosamine with a similar H···O distance of 2.0 Å. Although they have very different constraints, hydrogen bonds C and D have similar bond lengths, so it is consistent that they have a similar frequency.

Hydrogen bond E is found in the σ five-membered ring on the GP ring. SnH^+ involves only this type of IaHB among its four hydroxyls. Comparison of our SnH^+ spectra with those of gas-phase β-phenyl-D-glucoside measured by Simons and co-workers[27,42] offers some insight because neither of these structures have strong noncovalent interring bonding. We note the close agreement between the lowest energy conformers we calculate for SnH^+ and those of the phenyl-glucoside determined by Simons. Our SnH^+ experimental spectrum has a three times larger spread in the frequencies of the σ bands than that in phenyl-glucoside (45 and 15 cm^{-1} respectively). While Simons indicates that the presence of the phenyl ring does not influence the frequency of their observed GP-ring OH bands, it appears that proximity to the coumarin cation system leads to a larger spread of σ-frequencies. Comparing hydrogen bonds C and E, these have in common a five atom ring closed by the HB, but the planar constraint on type C permits a shorter H···O bond distance according to our models and a ~100 cm^{-1} larger red shift according to our spectrum.

That the OH vibration is influenced by its environment is further illustrated by $\gamma6$. This non-hydrogen-bonded OH present in EtH^+ (3648 cm^{-1}) and $EtNa^+$ (3661 cm^{-1}) is a substituent on a conjugated ring, in contrast to an OH on the GP ring. These lines have a 30 and 20 cm^{-1} red shift, respectively, from a free, gas-phase, alcoholic OH and are similar to phenyl-ring OH vibrational frequencies reported by Stearns[44] and Pillsbury.[45] The Supporting Information contains further discussion of the influence of conjugated systems on vicinal OH frequencies. Furthermore, our B3LYP modeling supports the identification of the 3633 cm^{-1} as the $\gamma7$ line in EnNa+. In this case, the oxygen in OH7 is coordinated to Na^+, raising the possibility that this noncovalent interaction accounts for some of the nearly 50 cm^{-1} red shift of this line. Applying our technique to deuterium-substituted $EnNa^+$ would replace the acidic OH7 with OD7 and shift the $\gamma7$ line out of the range of the σ lines allowing confirmation of the $\gamma7$ assignment.

The very strong, interring hydrogen bonding indicated by the red-shifted $\gamma7$ band in the EnH^+ spectrum suggests that experimental investigation of other naturally produced glycosides may shed more light on this interring bonding. The esculetin-7-*O*-glucoside, an isomer of esculin also known as chicorin, substitutes the GP ring in the 7-position rather than the 6-position, presenting the possibility of forming an interring IaHB involving an OH6 donor to a sugar OH. Daphnetin-8-*O*-glucoside, the glycoside of daphnetin (7,8-dihydroxycoumarin), has the potential to form an interring IaHB analogous to esculin. The glucoside of isoscopoletin (6-hydroxy-7-methoxycoumarin) substitutes the GP ring in the 6-position like esculin but lacks the OH7 required for interring bonding.

Provided the gas-phase structures are fully thermalized in the cooling process, one expects that the calculated lowest energy conformer will correspond to the most stable molecular structure observed in the experiment. However, the lowest energy conformer can be different in solution and in the gas phase and may be kinetically trapped through quenching collisions before they can surpass the corresponding potential energy barriers and reach the thermodynamically most stable gas-phase structure.[17,39] The importance of this effect will increase with molecular size because isomerization rates will be lower, and thus it is expected to affect more substantially the coumarin glycosides.

The sodiated glycosides, $EnNa^+$ and $SnNa^+$, have a chelated structure that constrains the orientation between the ring systems and can disrupt the clockwise σ-HB chain of the GP ring. While the conformers described in detail in the supporting information do not provide the exact match to our IR spectrum that we are seeking, they can be characterized as quite similar and we can observe that the tetradentate coordination tends to provide lower RMSD, suggesting better agreement with the experimental spectrum compared to tridentate conformers. In fact, all of the low energy conformers for $EnNa^+$ are tetradentate except for one, which has the poorest spectral match. A limitation of our modeling approach may be related to the challenge of applying the B3LYP functional to the large number of noncovalent interactions observed in our sodiated conformers. In a study involving sodiation similar to ours, Voss et al. use action spectroscopy to investigate the interaction of sodium ions with both anomers of glucose, and they observe multiple stable conformers. We note that several of their observed conformers have a six-member ring closed by a hydrogen bond with a frequency near 3400 cm^{-1}, consistent with our type D hydrogen bond. This serves to highlight one of the more remarkable features of this work, which is that the spectra point to observing just one conformer for each of the glycoside cations.

■ CONCLUSIONS

Inter- and intramolecular hydrogen bonding plays an essential role in determining the photophysics of coumarin-based fluorophores. This paper reports on the investigation of four characteristic coumarins, the two aglycone coumarins esculetin (Et) and scopoletin (St), as well as their glycoside derivatives, esculin (En) and scopolin (Sn). Using a combination of tandem mass spectrometry and cryogenic messenger-tagging infrared spectroscopy, vibrational transitions in the O−H stretch region are obtained for the protonated and sodiated species. The infrared spectra show a series of distinct vibrational bands corresponding to different types of O−H oscillators. Certain assignments can be deduced from the spectra by direct comparison, for example, revealing that the protonation site is on the carbonyl and that the N_2 tag hydrogen bonds to this OH. To assign the experimentally obtained infrared bands, theoretical evaluation of the relative stability and vibrational frequencies is performed on a series of conformers for each molecular ion. For all glycosides, this includes thorough investigation of the conformational space around the two dihedral angles that characterize the glycosidic bond and the relative orientation of the coumarin and glucopyranose planes. We find substantial agreement between theory and experiment, allowing us to assign all bands to different types of hydrogen bonding. The computational results confirm that slight structural changes in these coumarin derivatives have a dramatic effect on their hydrogen bonding patterns and support the ability of cryogenic infrared spectroscopy to identify subtle hydrogen bonding patterns in biomolecular ions. The measured spectra also provide an important benchmark for computational methods toward obtaining the energy and vibrational frequencies of such complex molecular species. Our results show that for the gas-phase cations of esculetin (EtH^+ and $EtNa^+$) and protonated esculin (EnH^+), the photoacidic OH7 is involved in intramolecular hydrogen bonding, and the latter exhibits a strong interring interaction. Future cryogenic infrared spectroscopy studies on selected gas phase coumarins, including microsolvated structures as well as on the anionic derivatives of these species, will further help understanding the strong hydrogen bonding interactions of these ions.

■ ASSOCIATED CONTENT

Supporting Information

The Supporting Information is available free of charge at https://pubs.acs.org/doi/10.1021/acs.jpca.0c06430.

> Arrival time distribution for ion mobility spectroscopic analysis of EnH+, table of experimental lines and calculated vibrational frequencies, scheme illustrating glycosidic dihedral angles and hydroxyl orientation, table showing EnH+ conformers, table of glycoside E_0 single-point energies, figures of all calculated glycoside spectra and accompanying tables of structural information, discussion of phenyl-bound OH vibrations, and cartesian coordinates of calculated glycoside structures.(PDF)

■ AUTHOR INFORMATION

Corresponding Author

Mark A. Muyskens − *Department of Chemistry and Biochemistry, Calvin University, Grand Rapids, Michigan 49546, United States;* orcid.org/0000-0001-6315-4515; Email: mark.muyskens@calvin.edu

Authors

Eduardo Carrascosa − *Laboratoire de Chimie Physique Moléculaire, École Polytechnique Fédérale de Lausanne, EPFL, CH-1015 Lausanne, Switzerland;* orcid.org/0000-0003-4338-8669

Robert P. Pellegrinelli − *Laboratoire de Chimie Physique Moléculaire, École Polytechnique Fédérale de Lausanne, EPFL, CH-1015 Lausanne, Switzerland*

Thomas R. Rizzo − *Laboratoire de Chimie Physique Moléculaire, École Polytechnique Fédérale de Lausanne, EPFL, CH-1015 Lausanne, Switzerland;* orcid.org/0000-0003-2796-905X

Complete contact information is available at: https://pubs.acs.org/10.1021/acs.jpca.0c06430

Author Contributions

[‖]M.A.M. and E.C. contributed equally to this work.

Notes

The authors declare no competing financial interest.

■ ACKNOWLEDGMENTS

The authors thank following members of the Rizzo Group that helped setting up the experiments and with the data acquisition: Irina Diukova, Ahmed Ben-Faleh, Stephan Warnke, and Natalia Yarlovenko. We thank the European Research Council (Grant 788697-GLYCANAL), the Swiss National Science Foundation through grant 200020_184838, and the EPFL for the financial support of this work. The computational modeling is supported in part by National Science Foundation MRI-grant 1726260 based at Calvin University, Grand Rapids, MI, USA. We acknowledge Calvin University for Calvin Research Fellowship support (MM).

■ REFERENCES

(1) Cao, D.; Liu, Z.; Verwilst, P.; Koo, S.; Jangjili, P.; Kim, J. S.; Lin, W. Coumarin-Based Small-Molecule Fluorescent Chemosensors. *Chem. Rev.* **2019**, *119*, 10403−10519.

(2) Gnonlonfin, G. J. B.; Sanni, A.; Brimer, L. Review Scopoletin - A Coumarin Phytoalexin with Medicinal Properties. *Crit. Rev. Plant Sci.* **2012**, *31*, 47−56.

(3) El Modafar, C.; Clerivet, A.; Fleuriet, A.; Macheix, J. J. Inoculation of *Platanus Acerifolia* with *Ceratocystis Fimbriata F. Sp. Platani* Induces Scopoletin and Umbelliferone Accumulation. *Phytochemistry* **1993**, *34*, 1271−1276.

(4) Penta, S. Introduction to Coumarin and SAR. In *Advances in Structure and Activity Relationship of Coumarin Derivatives*; Academic Press: Boston, 2016; 1−8.

(5) Kostova, I.; Bhatia, S.; Grigorov, P.; Balkansky, S.; Parmar, V. S.; Prasad, A. K.; Saso, L. Coumarins as Antioxidants. *Curr. Med. Chem.* **2011**, *18*, 3929−3951.

(6) Kirsch, G.; Abdelwahab, A. B.; Chaimbault, P. Natural and Synthetic Coumarins with Effects on Inflammation. *Molecules* **2016**, *21*, 1322.

(7) Mousa, S. A. Anticoagulants in Thrombosis and Cancer: The Missing Link. *Semin. Thromb. Hemostasis* **2002**, *28*, 45−52.

(8) Pham, H. T.; Yoo, J.; Vanden Berg, M.; Muyskens, M. A. Fluorescence of Scopoletin Including Its Photoacidity and Large Stokes Shift. *J. Fluoresc.* **2020**, *30*, 71−80.

(9) Moriya, T. Excited-State Reactions of Coumarins in Aqueous Solutions. I. The Phototautomerization of 7-Hydroxycoumarin and Its Derivative. *Bull. Chem. Soc. Jpn.* **1983**, *56*, 6−14.

(10) Simkovitch, R.; Huppert, D. Photoprotolytic Processes of Umbelliferone and Proposed Function in Resistance to Fungal Infection. *J. Phys. Chem. B* **2015**, *119*, 14683−14696.

(11) Duval, R.; Duplais, C. Fluorescent Natural Products as Probes and Tracers in Biology. *Nat. Prod. Rep.* **2017**, *34*, 161−193.

(12) Tattini, M.; Di Ferdinando, M.; Brunetti, C.; Goti, A.; Pollastri, S.; Bellasio, C.; Giordano, C.; Fini, A.; Agati, G. Esculetin and Esculin (Esculetin 6-O-Glucoside) Occur as Inclusions and Are Differentially Distributed in the Vacuole of Palisade Cells in Fraxinus Ornus Leaves: A Fluorescence Microscopy Analysis. *J. Photochem. Photobiol. B* **2014**, *140*, 28−35.

(13) Herschbach, D. R. Molecular Dynamics of Elementary Chemical Reactions (Nobel Lecture). *Angew. Chem., Int. Ed. Engl.* **1987**, *26*, 1221−1243.

(14) Levy, D. H. Laser Spectroscopy of Cold Gas-Phase Molecules. *Annu. Rev. Phys. Chem.* **1980**, *31*, 197−225.

(15) Ahmed, M.; Daly, S.; Dessent, C.; Dopfer, O.; Gabelica, V.; Gaigeot, M.-P.; Gatchell, M.; Gerber, B.; Gibbard, J.; Johnson, C.; et al. Going Large (r): General Discussion. *Faraday Discuss.* **2019**, *217*, 476−513.

(16) Rizzo, T.; Boyarkin, O. Cryogenic Methods for the Spectroscopy of Large, Biomolecular Ions. *In Gas-Phase IR Spectroscopy and Structure of Biological Molecules. Topics in Current Chemistry.*; Springer, Cham, 2014; *364*, 43−97.

(17) Voronina, L.; Masson, A.; Kamrath, M.; Schubert, F.; Clemmer, D.; Baldauf, C.; Rizzo, T. Conformations of Prolyl−Peptide Bonds in the Bradykinin 1−5 Fragment in Solution and in the Gas Phase. *J. Am. Chem. Soc.* **2016**, *138*, 9224−9233.

(18) Okumura, M.; Yeh, L. I.; Myers, J. D.; Lee, Y. T. Infrared Spectra of the Solvated Hydronium Ion: Vibrational Predissociation Spectroscopy of Mass-Selected $H_3O^+{\cdot}(H_2O)_n{\cdot}(H_2)_m$. *J. Phys. Chem.* **1990**, *94*, 3416−3427.

(19) Heine, N.; Asmis, K. R. Cryogenic Ion Trap Vibrational Spectroscopy of Hydrogen-Bonded Clusters Relevant to Atmospheric Chemistry. *Int. Rev. Phys. Chem.* **2014**, *34*, 1−34.

(20) Kamrath, M. Z.; Garand, E.; Jordan, P. A.; Leavitt, C. M.; Wolk, A. B.; Van Stipdonk, M. J.; Miller, S. J.; Johnson, M. A. Vibrational Characterization of Simple Peptides Using Cryogenic Infrared Photodissociation of H_2-Tagged. *Mass-Selected Ions. J. Am. Chem. Soc.* **2011**, *133*, 6440−6448.

(21) Garand, E.; Kamrath, M. Z.; Jordan, P. A.; Wolk, A. B.; Leavitt, C. M.; McCoy, A. B.; Miller, S. J.; Johnson, M. A. Determination of Noncovalent Docking by Infrared Spectroscopy of Cold Gas-Phase Complexes. *Science* **2012**, *335*, 694−698.

(22) Svendsen, A.; Lorenz, U. J.; Boyarkin, O. V.; Rizzo, T. R. A New Tandem Mass Spectrometer for Photofragment Spectroscopy of Cold, Gas-Phase Molecular Ions. *Rev. Sci. Instrum.* **2010**, *81*, No. 073107.

(23) Ben Faleh, A.; Warnke, S.; Rizzo, T. R. Combining Ultrahigh-Resolution Ion-Mobility Spectrometry with Cryogenic Infrared Spectroscopy for the Analysis of Glycan Mixtures. *Anal. Chem.* **2019**, *91*, 4876−4882.

(24) Gidden, J.; Bowers, M. T. Gas-Phase Conformations of Deprotonated and Protonated Mononucleotides Determined by Ion Mobility and Theoretical Modeling. *J. Phys. Chem. B* **2003**, *107*, 12829−12837.

(25) Frisch, M.; Trucks, G.; Schlegel, H.; Scuseria, G.; Robb, M.; Cheeseman, J.; Montgomery, J.; Vreven, T.; Kudin, K.; Burant, J.; et al. Gaussian 16, Revision B.01; Gaussian, Inc.: Wallingford, CT, 2016.

(26) Schmidt, J.; Polik, W. WebMO Enterprise, version 20.0. WebMO, LLC, Holland, MI, USA. http: //www.webmo.net (accessed 2020).

(27) Simons, J. P.; Jockusch, R. A.; ÇarÇabal, P.; Hünig, I.; Kroemer, R. T.; Macleod, N. A.; Snoek, L. C. Sugars in the Gas Phase. Spectroscopy, Conformation, Hydration, Co-Operativity and Selectivity. *Int. Rev. Phys. Chem.* **2005**, *24*, 489−531.

(28) Simons, J. P. Good Vibrations: Probing Biomolecular Structure and Interactions through Spectroscopy in the Gas Phase. *Mol. Phys.* **2009**, *107*, 2435−2458.

(29) Becke, A. D. Density-Functional Exchange-Energy Approximation with Correct Asymptotic Behavior. *Phys. Rev. A* **1988**, *38*, 3098.

(30) Becke, A. D. Density-Functional Thermochemistry. III. The Role of Exact Exchange. *J. Chem. Phys.* **1993**, *98*, 5648.

(31) Lee, C.; Yang, W.; Parr, R. G. Development of the Colle-Salvetti Correlation-Energy Formula into a Functional of the Electron Density. *Phys. Rev. B* **1988**, *37*, 785.

(32) Grimme, S.; Ehrlich, S.; Goerigk, L. Effect of the Damping Function in Dispersion Corrected Density Functional Theory. *J. Comput. Chem.* **2011**, *32*, 1456−1465.

(33) Boys, S. F.; Bernardi, F. The Calculation of Small Molecular Interactions by the Differences of Separate Total Energies. Some Procedures with Reduced Errors. *Mol. Phys.* **2006**, *19*, 553−566.

(34) Johnson, R. D. NIST Computational Chemistry Comparison and Benchmark Database, NIST Standard Reference Database Number 101 Release 20 http://cccbdb . nist.gov/ (accessed Oct 15, 2020).

(35) Katari, M.; Nicol, E.; Steinmetz, V.; van der Rest, G.; Carmichael, D.; Frison, G. Improved Infrared Spectra Prediction by DFT from a New Experimental Database. *Chem. − Eur. J.* **2017**, *23*, 8414−8423.

(36) Masellis, C.; Khanal, N.; Kamrath, M. Z.; Clemmer, D. E.; Rizzo, T. R. Cryogenic Vibrational Spectroscopy Provides Unique Fingerprints for Glycan Identification. *J. Am. Soc. Mass Spectrom.* **2017**, *28*, 2217−2222.

(37) Voss, J. M.; Kregel, S. J.; Fischer, K. C.; Garand, E. IR-IR Conformation Specific Spectroscopy of Na+(Glucose) Adducts. *J. Am. Soc. Mass Spectrom.* **2018**, *29*, 42−50.

(38) Huisken, F.; Kulcke, A.; Laush, C.; Lisy, J. M. Dissociation of Small Methanol Clusters after Excitation of the O−H Stretch Vibration at 2.7 μ. *J. Chem. Phys.* **1991**, *95*, 3924−3929.

(39) Voronina, L.; Rizzo, T. R. Spectroscopic Studies of Kinetically Trapped Conformations in the Gas Phase: The Case of Triply Protonated Bradykinin. *Phys. Chem. Chem. Phys.* **2015**, *17*, 25828−25836.

(40) Baldauf, C.; Pagel, K.; Warnke, S.; von Helden, G.; Koksch, B.; Blum, V.; Scheffler, M. How Cations Change Peptide Structure. *Chem. − Eur. J.* **2013**, *19*, 11224−11234.

(41) Struwe, W. B.; Baldauf, C.; Hofmann, J.; Rudd, P. M.; Pagel, K. Ion Mobility Separation of Deprotonated Oligosaccharide Isomers− Evidence for Gas-Phase Charge Migration. *Chem. Commun.* **2016**, *52*, 12353−12356.

(42) Jockusch, R. A.; Kroemer, R. T.; Talbot, F. O.; Snoek, L. C.; ÇCaŗabal, P.; Simons, J. P.; Havenith, M.; Bakker, J. M.; Compagnon, I.; Meijer, G.; et al. Probing the Glycosidic Linkage: UV and IR Ion-Dip Spectroscopy of a Lactoside. *J. Am. Chem. Soc.* **2004**, *126*, 5709−5714.

(43) Scutelnic, V.; Rizzo, T. R. Cryogenic Ion Spectroscopy for Identification of Monosaccharide Anomers. *J. Phys. Chem. A* **2019**, *123*, 2815−2819.

(44) Stearns, J. A.; Mercier, S.; Seaiby, C.; Guidi, M.; Boyarkin, O. V.; Rizzo, T. R. Conformation-Specific Spectroscopy and Photodissociation of Cold, Protonated Tyrosine and Phenylalanine. *J. Am. Chem. Soc.* **2007**, *129*, 11814−11820.

(45) Pillsbury, N. R.; Stearns, J. A.; Müller, C. W.; Plusquellic, D. F.; Zwier, T. S. State-Specific Studies of Internal Mixing in a Prototypical Flexible Bichromophore: Diphenylmethane. *J. Chem. Phys.* **2008**, *129*, 114301.